Age-Optimal Network Coding HARQ Scheme for Satellite-Based Internet of Things

Jing Ding, Jian Jiao, *Member, IEEE*, Jianhao Huang, Shaohua Wu, *Member, IEEE*, Rongxing Lu, *Fellow, IEEE*, and Qinyu Zhang, *Senior Member, IEEE*

***Abstract*—Satellite-based Internet of Things (S-IoT) is viewed as an efficient solution to provide timely status updates to the terrestrial user equipment (UE), due to its ubiquitous coverage and broadband access capability inherited from high throughput satellite (HTS). However, the conventional hybrid automatic repeat request (HARQ) cannot guarantee the freshness of status update transmission, because the reliable transmission needs the retransmission of the lost packets, which deteriorates the freshness due to the nontrivial propagation delay and high bit error rate (BER) of the satellite–territory link (STL). In this article, we propose an age-optimal network coding HARQ (NC HARQ) scheme with the metric of information timeliness, i.e., Age of Information (AoI) to realize timely status updates in S-IoT. First, we model the STL as a shadowed Rician (SR) fading channel and derive the closed-form expressions of BER. Then, we propose a fixed interval NC inserted HARQ (f-NC HARQ) scheme, where the NC packets are inserted in the information packets with fixed interval to accelerate the recovery of lost information packets and derive the expressions of Peak AoI (PAoI) and average end-to-end delay. Furthermore, we propose an adaptive NC inserted HARQ (A-NC HARQ) scheme for the drastic variations in the SR fading channel, where the transmission of the status update is modeled as a partially observable Markov decision process (POMDP) problem and solved by a low complexity improved fast informed bound (iFIB) algorithm. Simulation results validate the accuracy of our theoretical derivations and show that the A-NC HARQ scheme can achieve the lowest PAoI and average end-to-end delay.**

***Index Terms*—Age of Information (AoI), hybrid automatic request, partially observable Markov decision process (POMDP), Satellite-based Internet of Things (S-IoT), shadowed-Rician fading channel.**

Manuscript received 31 March 2022; revised 29 April 2022; accepted 6 June 2022. Date of publication 10 June 2022; date of current version 24 October 2022. This work was supported in part by the National Natural Science Foundation of China (NSFC) under Grant 62071141, Grant 61871147, Grant 61831008, and Grant 62027802; in part by the Natural Science Foundation of Guangdong Province under Grant 2020A1515010505; in part by the Guangdong Science and Technology Planning Project under Grant 2018B030322004; in part by the Shenzhen Science and Technology Program under Grant ZDSYS20210623091808025 and Grant GXWD20201230155427003-20200822165138001; and in part by the Major Key Project of PCL under Grant PCL2021A03-1. *(Corresponding author: Jian Jiao.)*

Jing Ding, Jian Jiao, Jianhao Huang, Shaohua Wu, and Qinyu Zhang are with the Communication Engineering Research Centre, Harbin Institute of Technology (Shenzhen), Shenzhen 518055, China, and also with Peng Cheng Laboratory, Shenzhen 518055, China (e-mail: 20S152068@stu.hit.edu.cn; jiaojian@hit.edu.cn; 180210220@stu.hit.edu.cn; hitwush@hit.edu.cn; zqy@hit.edu.cn).

Rongxing Lu is with the Faculty of Computer Science, University of New Brunswick, Fredericton, NB E3B 5A3, Canada (e-mail: rlu1@unb.ca).

Digital Object Identifier 10.1109/JIOT.2022.3182006

I. Introduction

INTERNET of Things (IoT) has been widely applied to various applications due to its capability to enable ubiquitous connections. As an important branch of IoT, Satellite-based IoT (S-IoT) is a promising solution to provide seamless communication coverage for a wide geographic area and extreme terrain [1]. Moreover, with the development of IoT devices and S-IoT applications, information freshness is an urgent requirement in various status update systems, such as environmental monitoring, smart grid, emergency management [2]–[4], etc., which need real-time information updates.

Since the information freshness is affected not only by the transmission delay but also by the generation interval in S-IoT, traditional packet-centric metrics, such as average delay and throughput, cannot fully characterize freshness [5]. In order to capture the feature of information freshness, a new metric named Age of Information (AoI) was originally introduced in [6], which is defined as the time elapses since the last received update is generated at the source. Therefore, information packets need the reliable end-to-end transmission in S-IoT with low-Earth orbits (LEOs) high throughput satellite (HTS) to guarantee the freshness, since the loss of packets may need retransmission, which will significantly decrease the freshness due to the nontrivial propagation delay between LEO HTS and user equipment (UE). To further enhance the reliability, we introduce a network coding hybrid automatic repeat request (NC HARQ) to recover lost packets with redundant NC packets and avoid retransmission [7]. Moreover, the information packets need to be recovered at the receiver in time to further improve their AoI. Hence, a tradeoff can be found between the number of NC packets for reliable transmission and guarantee the freshness without leading to extra transmission delay and energy. In addition, the positions to insert the NC packets can significantly affect the freshness, which should be carefully designed in the NC HARQ scheme.

A. Related Works

Abdi *et al.* [8] modeled the satellite–territory link (STL) as the shadowed Rician (SR) channel and derived an accurate expression of the probability density function (PDF) of instantaneous power, which provide a widely used STL channel model and has been extensively studied in the physical layer design, such as the derivation of outage probability and ergodic capacity [9], [10]. Moreover, [11] presents an approximate expression of bit error rate (BER) with a large

signal-to-noise ratio (SNR), and [12] analyzes and derives an approximate BER expression in multiple-input and multiple-output (MIMO) system by approximating the nonintegrable integral with moment generating function (MGF). To precisely describe the performance of physical layer forward error correction (FEC) codes in S-IoT, we need to derive a more accurate BER for the SR fading channel.

Furthermore, the bit-level FEC codes cannot guarantee the reliable transmission due to the high BER in STL, even they have approached the Shannon limit [13], and the failure decoded packets are viewed as lost at the transport layer and request retransmission. To address this issue, the Consultative Committee for Space Data Systems (CCSDS) released the long erasure code (LEC) specification to perform a packet-level LEC at the transport layer [14], and the receiver can recover the lost packets by utilizing the received redundant LEC packets and avoid retransmission. Xu *et al.* [15] and Karzand *et al.* [16] proved that LEC can effectively resolve the packet loss and lower the end-to-end delay. Moreover, the NC has attracted considerable research interests to address the throughput bottleneck in satellite–terrestrial communications [17], [18]. Jiao *et al.* [7] have proved that the NC HARQ can achieve a better energy-efficient performance compared with traditional hybrid automatic repeat request (HARQ). Liu *et al.* [19] have proved that the NC HARQ can achieve lower delay and AoI compared with several state-of-the-art HARQ schemes in S-IoT. However, the number of NC packets for reliable transmission in SR channel without leading extra transmission delay and energy is still missing.

Moreover, AoI is a destination-centric metric that only focuses on the latest status update at the receiver and is an alternative performance metric in the time-sensitive wireless communication system [20], [21]. The optimization of AoI and delay has been proved is contradictory when the service time follows the heavy tail distribution in [22] and [23]. Moreover, a status update may consist of multiple packets, and the Average AoI (AAoI) of packets cannot exactly characterize the freshness of the status update. Note that the Peak AoI (PAoI) describes the maximum value of AoI in each status update transmission, which can capture the recovery of the last packet in a status update [24]–[27]. Therefore, the PAoI is introduced in our S-IoT system to characterize the freshness and the extent to which the status update is stale. Furthermore, the information packets will be backlogged by previously lost packets at the UE in the conventional NC HARQ scheme, and lead to larger PAoI for waiting the NC packets to recover the previously lost packets. Hence, how to insert the NC packets in the status update and decrease the PAoI in the end-to-end S-IoT transmission is required for further study.

B. Contributions

In this article, we propose an age-optimal NC HARQ scheme for S-IoT and analyze the PAoI of the end-to-end status update transmission with multiple packets. Specifically, the main contributions are as follows.

1) We model the STL as the SR fading channel and derive an accurate closed-form expression of BER with a single antenna, which can significantly lower the computational complexity and provide more accurate results compared to the existing approximate BER expressions. To the best of our knowledge, this is the first work to derive a closed-form expression of BER in SR fading channel. Moreover, considering the practical usage of MIMO in STL [28], we further derive the BER over the SR channel in the MIMO system.
2) We utilize NC as LEC to encode the packets in each status update and propose an age-optimal NC HARQ scheme for S-IoT. With the help of our derived BER expressions, we can predetermine an appropriate number of NC packets to recover the lost information packets and avoid retransmission in the variable SR channel. Then, we design a fixed interval NC inserted HARQ (f-NC HARQ) scheme, where the NC packets will be inserted in the information packets with a fixed interval to accelerate the recovery of lost information packets, and derive the closed-form expression of PAoI and an approximation of average end-to-end delay of the f-NC HARQ scheme. Simulation results show that there is an optimal fixed insertion interval in different SNRs in the variable SR fading channel.
3) We propose an adaptive NC inserted HARQ (A-NC HARQ) scheme to optimize the PAoI and average end-to-end delay. The transmission of the status update is first modeled as a partially observable Markov decision process (POMDP) problem in the variable SR channel, where the HTS predicts the channel status with delayed feedback negative acknowledgment (NAK) from the UE or without feedback and decides to transmit the information packet or NC packet. This POMDP problem is solved by an improved fast informed bound (iFIB) algorithm. Finally, simulation results validate the accuracy of our theoretical derivations and show that the A-NC HARQ scheme can outperform the f-NC HARQ scheme.

C. Outline

The remainder of this article is organized as follows. In Section II, we describe the system model and derive the closed-form expression of BER over the SR fading channel. In Section III, we analyze the PAoI and average end-to-end delay in the f-NC HARQ scheme. In Section IV, we propose the A-NC HARQ scheme based on POMDP and solve it by a low complexity iFIB algorithm. Simulation results are presented in Section V. Finally, Section VI draws the conclusion.

II. System Model and NC HARQ Scheme

An end-to-end transmission in S-IoT as shown in Fig. 1, where a LEO HTS collects status updates and transmits them to the corresponding UEs over an error-prone channel with a nontrivial propagation delay. Note that the status updates are age-critical, which means the length of the status updates is relatively small, and usually corresponding to several finite block-length packets in a file. Assume that each status update includes k information packets, and these information packets

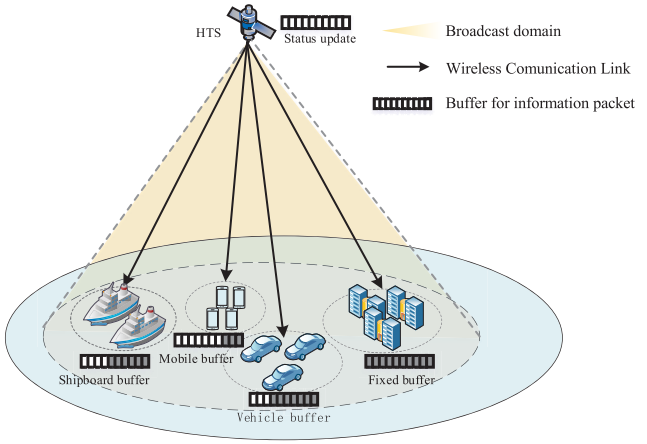

Fig. 1. Illustration of the S-IoT transmission scenario.

TABLE I
RELEVANT NOTATION

notation	Definition
k	The number of packets in a status update
B	The packet size
N	The number of antennas
Ω	The average power of LoS component
$2b_0$	The average power of the multipath component
m	The parameter of fading severity of the channel
$\overline{\gamma}$	The average value of signal noise ratio
r	The instantaneous signal noise ratio
γ	The average value of signal noise ratio
r	The instantaneous signal noise ratio
t_r	The prorogation delay
t_s	The transmission delay
W_q	The queueing time
W_s	The service time
S	The system state set
$s_{t,\iota}$	The system state at time t
Z	The system observation set
z_{t-t_r}	The system observation at time t
$\mathcal{A}$	The action set of HTS

are temporarily buffered at the HTS and wait for transmission in order. At the UE side, the ith information packet is temporarily buffered at the transport layer. If the previous 1 to $i-1$ information packets are successfully received, the ith information packet will be uploaded to the application layer. Otherwise, it waits for the successful recovery of the previously lost information packets. For convenience, we introduce the related notations in Table I.

Without loss of generality, we assume that the duration of one time slot equals to the transmission delay t_s for a packet, and t_r denotes the prorogation delay. Moreover, since the distance between the HTS and UEs is more than several hundred kilometers, the Doppler shifts caused by the motion of HTS are identical for different UEs in a same spot beam [29]. Furthermore, the bandwidth of HTS is about 800 MHz to 2 GHz, we can set the guard bandwidth as double as the Doppler shifts, and the influence of Doppler shifts on the system can be relieved [30].

Note that our NC HARQ can be viewed as an incremental-redundancy (IR) HARQ, where each NC packet is assumed to help recovering one previously lost information packet as shown in Fig. 2. Let d_i $(i = 1, 2, \ldots, k)$ denote the ith information packet, and $C_j (j = 1, 2, \ldots,)$ denote the jth NC packet. Thus, C_j is constructed by random linear network coding (RLNC) of all the previous u $(u = \min(u, k))$ transmitted information packets as follows [16]:

$$C_j = f_j(d_1, d_2, \ldots, d_u) = \sum_{i=1}^{u} w_{ij} d_i \tag{1}$$

where d_i is viewed as a vector in a finite field GF(q) with order q, and each coefficient w_{ij} is randomly selected from GF(q). Moreover, the UE maintains a generator matrix G_t at time slot t, which is composed of the coefficients of received packets. If G_t is full rank, i.e., the number of available packets at UE equals to that of the transmitted information packets, the Gaussian elimination can be used to recover the lost information packets. Furthermore, the SNR range of channel status information (CSI) can be estimated from the receiving signals and informed within 2–3 bits in the acknowledgment (ACK) or NAK [31], [32]. When UE receives the last packet from HTS, it sends an ACK or NAK to HTS to inform the current channel CSI and whether the retransmission is needed [33].

A. f-NC HARQ Scheme

In this section, we propose the f-NC HARQ scheme, where each NC packet is inserted into the k information packets with equal interval L during the transmission of a status update. A detailed example in Fig. 2(a) is introduced as follows.

Specifically, we assume that the status update at HTS includes $k = 6$ information packets at time slot $t = 0$ and L is estimated as $L = 3$. In the first status update transmission, d_1 and d_2 are uploaded to the application layer immediately when they are received successfully at UE, and the NC packet C_1 is useless because there is no lost information packet. Next, d_3 is lost at $t = 5$, and although d_4 is successfully received at $t = 6$, it cannot upload to the application layer. Then, when C_2 is successfully received at $t = 7$, it can recover one lost information packet as $C_2 = f_2(d_1, d_2, d_3, d_4)$, and d_3 is recovered. Thus, d_3 and d_4 upload to the application layer after $t = 7$. Finally, d_5 is received and uploaded to the application layer at $t = 8$, and the lost information packet d_6 is recovered by C_3 at $t = 10$. Therefore, all six information packets have been recovered and the UE sends an ACK to the HTS to inform the current CSI and waits for the second status update.

In the second status update transmission as shown in Fig. 2(a), we can observe that d_1 is received at $t = 2$ and d_2 is recovered at $t = 4$ via C_1. Next, d_3 and d_4 fail to be received and C_2 succeeds at $t = 7$. However, one NC packet cannot recover two lost information packets. Then, d_5 and d_6 are successfully received but C_3 is lost, and UE still cannot recover d_3 and d_4, thus d_5 and d_6 are backlogged at the transport layer. Therefore, the UE sends a NAK to HTS to inform the current CSI and requests retransmission. Finally, the HTS sends two NC packets $C_4 = f_4(d_1, d_2, d_3, d_4, d_5, d_6)$

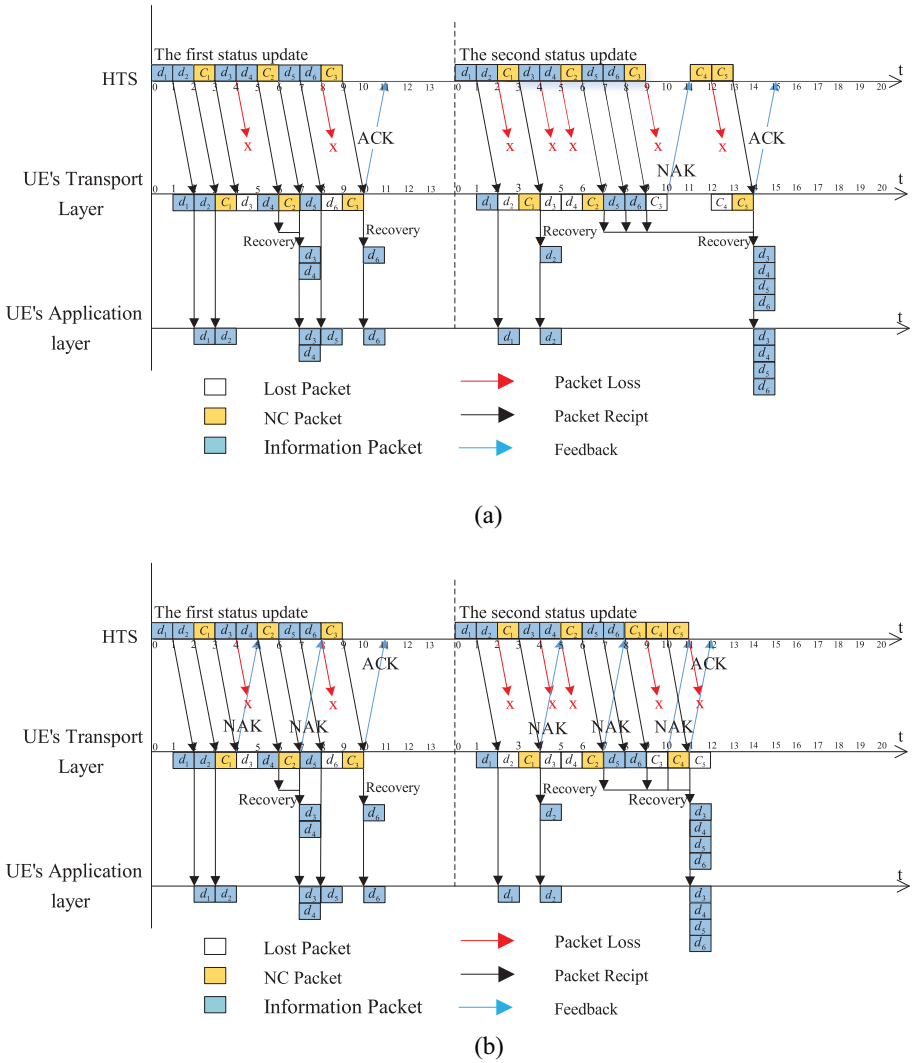

Fig. 2. Example of the end-to-end transmission of two status updates with NC HARQ with SNR = 9 dB. (a) Two status updates transmission with f-NC HARQ, where $k = 6$ and $L = 3$. (b) Two status updates transmission with A-NC HARQ, where $k = 6$ and $T = 3$.

and $C_5 = f_5(d_1, d_2, d_3, d_4, d_5, d_6)$ according to the CSI, and UE utilizes the successfully received C_5 to recover d_3 and d_4 with C_2 at $t = 14$, and all six information packets of second status update have been uploaded to the application layer in order.

Note that the HTS can only receive the delayed CSI due to the nontrivial propagation delay, and the SR fading channel randomly varies between two adjacent status update transmissions. As shown in Fig. 2(a), when the CSI turns to *bad* in the second status update, the predetermined $L = 3$ cannot provide sufficient NC packets to recover the lost information packets, and the HTS finds the failure of second status update transmission at $t = 12$ and transmits two NC packets C_4 and C_5 according to the delayed feedback NAK. This retransmission deteriorates the performance of average end-to-end delay, PAoI, and throughput in our end-to-end S-IoT transmission. Thus, two key challenges need to be addressed in the following, one is to derive a more accurate BER expression for the SR fading channel. The other is to design the A-NC HARQ to predict the channel status with delayed feedback and then switch an appropriate L to avoid retransmission.

B. A-NC HARQ Scheme

In this section, we propose the A-NC HARQ scheme to improve the transmission over block fading SR fading channel, where the UE can issue NAKs to the HTS in each T time slot as the asynchronous NAK mode in the CCSDS file delivery protocol (CFDP) [33], then the HTS can reselect an appropriate L according to the NAK to generate and transmit NC packets as shown in Fig. 2(b). Note that t_r and t_s equal to the duration of time slot in our system model, the most frequency of NAK is $T = 1$. An example A-NC HARQ scheme with $k = 6$ and $T = 3$ is shown in Fig. 2(b), where the channel condition is the same as that in Fig. 2(a).

In the first status update transmission, the AoI updates at $t = 10$ in the A-NC HARQ scheme since the first status update is

successfully recovered, which is identical to the f-NC HARQ scheme.

In the second status update transmission, d_3 and d_4 both fail to be received and the received NC packet C_2 at $t = 7$ cannot recover two lost information packets. Then, the HTS reselects L according to the feedback NAK at $t = 9$ and immediately transmits two NC packets $C_4 = f_4(d_1, d_2, d_3, d_4, d_5, d_6)$ and $C_5 = f_5(d_1, d_2, d_3, d_4, d_5, d_6)$. Thus, the UE utilizes the successfully received C_4 to recover d_3 and d_4 with C_2 at $t = 11$, and the backlogged d_5 and d_6 can be uploaded at $t = 11$. Therefore, the A-NC HARQ scheme can reduce 27% of time slot consumption than the f-NC HARQ scheme in the same channel condition with 3 NAKs as shown in Fig. 2.

Obviously, if we can model a more accurate block fading SR channel and design a related optimize transmission policy, the A-NC HARQ can reselect an appropriate L with less frequency NAK feedback. Note that in both f-NC HARQ and A-NC HARQ schemes, the HTS can calculate the required number of NC packets to ensure reliable transmission via the feedback CSI, there is no more than one retransmission in our NC HARQ scheme. Thus, we should derive a more accurate BER expression for the SR channel first.

C. BER Derivation of SR Fading Channel

The STL is modeled as the widely used SR fading channel in this article, and the PDF of instantaneous SNR r is given by [8]

$$f(r) = \frac{1}{2b_0\gamma}\left(\frac{2b_0 m}{2b_0 m + \Omega}\right)^m \exp\left(-\frac{r}{2b_0\gamma}\right) \cdot {}_1F_1\left(m, 1, \frac{1}{2b_0\gamma}\left(\frac{\Omega}{(2b_0 m + \Omega)}\right)r\right) \tag{2}$$

where ${}_1F_1(.,.,.)$ is the confluent hypergeometric function, γ denotes the average value of SNR, Ω is the average power of LoS component, $2b_0$ is the average power of the multipath component, and m ($m \geq 0$) is the parameter of channel fading severity.

In addition, the BER of M-PSK in additive white Gaussian noise (AWGN) channel is given by [34]

$$P_e(r) \cong \frac{2}{\zeta_M} \sum_{j=1}^{\max(M/4,1)} Q\left(\sqrt{2r}b_j\right) \tag{3}$$

where $Q(\cdot)$ represents the Q-function, $\zeta_M = \max(\log_2 M, 2)$ and $b_j = \sin([(2j-1)\pi]/M)$. Moreover, since r is variable for given γ in (2), and the corresponding instantaneous BER is also variable according to (3), the average BER in SR fading channel equals to the cumulative sum of BER for variable r, which can be expressed as

$$P_e(\gamma) = \int f(r)P_e(r)dr. \tag{4}$$

Note that Abdi *et al.* [8] proved that (2) has the first- and second-order statistics, which means (4) is integrable. Therefore, by substituting (2) and (3) into (4), and let Γ represent the Gamma function, $\alpha = [1/(2b_0\gamma)]([2b_0 m]/[2b_0 m + \Omega])^m$, $\eta = (m/[(2b_0 m + \Omega)\gamma])$, $\theta_k = ([(-1)^k(1-m)_k]/k!)([1/(2b_0\gamma)][\Omega/(2b_0 m + \Omega)])^k$, and $v = [(2i+1)/2]$, we derive the closed-form expression of BER with single antenna over SR channel as (5), shown at the bottom of the page, and the detailed derivation is given in Appendix A.

Furthermore, Arti and Jindal [35] proved that the MIMO gain at UE equals to the sum of N independent signal, i.e., $Z = X_1 + X_2 + \cdots + X_N$, where $N = N_r \times N_t$ is the diversity gain, and N_r and N_t are the number of receive and transmit antennas, respectively. Thus, the BER with the MIMO system in the SR fading channel can be derived as (6), shown at the bottom of the page, and the detailed derivation is given in Appendix B.

As shown in Fig. 3, the theory BER curves of (5) and (6), as shown at the bottom of this page match precisely with the simulated curves. However, since the SR fading channel is fast varying [36], the BER calculates from the average SNR cannot fully guarantee the reliable transmission as shown in Fig. 2(a). Thus, we design the A-NC HARQ scheme, where the HTS can predict the CSI via a POMDP

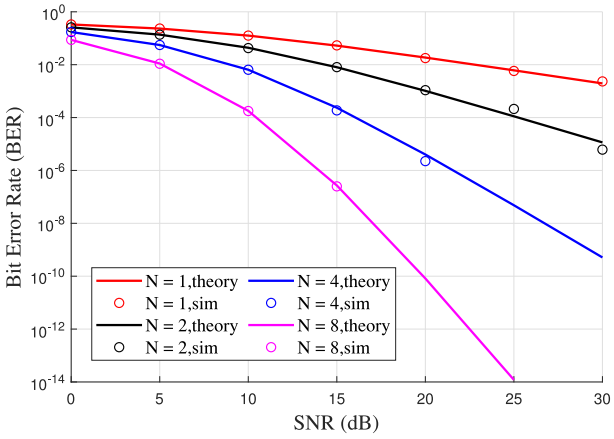

Fig. 3. Analytical and simulated BER with BPSK and different diversity gains.

$$P_e(\gamma) = \sum_{k=0}^{m-1} \alpha\theta_k \sum_{j=1}^{\max(M/4,1)} \frac{1}{\zeta_M}\left(\frac{1}{\eta^{k+1}} - \frac{1}{\sqrt{2\pi}}\sum_{i=0}^{k}\frac{1}{i!}\frac{1}{2^{i-v}b_j^{2i}\eta^{k-i+1}\left(1+\eta/b_j^2\right)^v}\Gamma(v)\right) \tag{5}$$

$$P_e(\gamma) = \alpha^N \sum_{j=1}^{\max(M/4,1)} \frac{1}{\zeta_M}\left(\frac{1}{\eta^N} - \frac{1}{\sqrt{2\pi}}\sum_{i=0}^{N-1}\frac{1}{i!}\frac{1}{2^{i-v}b_j^{2i}\eta^{N-i}\left(1+\eta/b_j^2\right)^v}\Gamma(v)\right) \tag{6}$$

optimization and reselects a proper L to avoid retransmission as shown in Fig. 2(b). Moreover, the detailed analysis of POMDP to design an optimal A-NC HARQ is introduced in Section IV.

III. Theoretical Analysis of f-NC Scheme

In this section, we mainly analyze the average end-to-end delay and PAoI of the f-NC HARQ scheme.

A. Average End-to-End Delay

Without loss of generality, we assume that the status update collected by HTS includes k ($k > 0$) information packets at $t = 0$. According to the transmission processes of the f-NC HARQ scheme as shown in Fig. 2, the end-to-end delay W_i of d_i ($i = 1, 2, \ldots, k$) can be divided into three parts.

1) *Queueing Delay W_q:* The elapsed time of the information packet from its generation at HTS to its transmission.
2) *Service Delay W_s:* The time elapses for the information packet since it is transmitted from the HTS until uploaded to the application layer at UE.
3) *Propagation Delay t_r:* The elapsed time of the information packet travels from the HTS to UE.

Hence, we have

$$W_i = W_q(i) + W_s(i) + t_r. \tag{7}$$

Then, when the HTS attempts to send d_i, there are $(i-1)$ information packets and $(\lceil i/(L-1) \rceil - 1)$ NC packets are already transmitted. Therefore, (7) can be further written as

$$W_i = \left(\left\lceil \frac{i}{L-1} \right\rceil - 1 + i - 1 \right) \cdot t_s + t_r + W_s(i) \tag{8}$$

where t_s is the transmission delay and we assume that $t_s = t_r$.

Therefore, the average end-to-end delay $\bar{W} = (1/k)\sum_{i=1}^{k} W_i$ for the f-NC HARQ scheme can be expressed as

$$\begin{aligned} \bar{W} &= \frac{1}{k}\sum_{i=1}^{k}\left(\left(\left\lceil \frac{i}{L-1} \right\rceil - 1 + i - 1 \right) \cdot t_s + t_r + W_s(i) \right) \\ &= \frac{1}{k}\left(\sum_{j=1}^{k/(L-1)} (L-1) \cdot \frac{(j-1)\cdot L + (j\cdot L - 2)}{2} \right) \cdot t_s \\ &\quad + t_r + \frac{1}{k}\sum_{i=1}^{k} W_s(i) \\ &= \frac{(k-2)L+4}{4(L-1)} \cdot t_s + t_r + \frac{1}{k}\sum_{i=1}^{k} W_s(i). \end{aligned} \tag{9}$$

Obviously, the first and second parts of (9) are constants. In addition, the third part of (9) is correlative with the CSI. Therefore, we introduce the concept of "busy/idle stage" into the sequential transmission for further analysis [16]. First, the "busy stage" refers to the time elapses since the sequential transmission is paused due to the lost information packets until that the sequential transmission resumes, e.g., as the second status update shown in Fig. 2(a), the busy stage is from $t = 5$ to $t = 16$. Defined χ as the number of transmitted NC packets during the busy stage, and the "idle stage" refers to the period of sequential delivery without pause, which can be expressed as $\chi = 0$. Since the packet loss is i.i.d., the busy/idle stage and the random variable χ are i.i.d., which is characterized by the probability distribution refers to [16]

$$h_\chi(x) = \begin{cases} (1-p)^{L-1}, & \text{for } x = 0 \\ (L-1)p(1-p)^{L-1}, & \text{for } x = 1 \\ \frac{L-1}{x} p^x (1-p)^{x(L-1)} C_{(x-1)L}^{x-1}, & \text{for } x > 1 \\ 0, & \text{otherwise} \end{cases} \tag{10}$$

where p is the block error rate (BLER), which can be calculated by the BER P_e and packet size B, as follows:

$$p = 1 - (1 - P_e)^B. \tag{11}$$

Then, we can get $E(\chi) = ([(L-1)p(1-p)^{L-1}]/[1 - L\cdot p])$, $E(\chi^2) = E(\chi) + ([L(L-1)p^2(1-p)^L]/[(1-L\cdot p)^3])$ and $E(\chi^+) = [(1-p)^L/(1-L\cdot p)]$.

Therefore, the element $\sum_{i=1}^{k} W_s(i)$ in (9) is the sum of service time in a status update, which equals to the sum of busy stage. When the BLER satisfies $L\cdot p < 1$, the expected of $\sum_{i=1}^{k} W_s(i)$ can be upper bounded as follows [16]:

$$\lim_{k\to\infty} \frac{1}{k} E\left(\sum_{i=1}^{k} W_s(i) \right) \le \frac{E(\chi^2)(L-1)}{2E(\chi^+)}. \tag{12}$$

Moreover, when $L\cdot p > 1$, the received NC packets cannot recover the lost information packets and UE will send NAK to request retransmission as the second status update shown in Fig. 2(b), and (12) is inaccurate when $L\cdot p > 1$. Considering that when $L\cdot p > 1$ and any busy stage starts, the transmission most likely does not return to the idle stage in this status update. Thus, k information packets can be divided into $[k/(L-1)]$ groups. The probability of a busy stage starts from the ith information packet in the $(l+1)$th group equals to $P_{out} = p(1-p)^{l(L-1)+i-1}$. In this situation, there are still $\Psi_{gr} = [k/(L-1)] - l - 1$ groups. Moreover, we can conclude that there are $\Psi_{tp} = \Psi_{gr} \cdot L + L - i$ packets and $\Psi_{ip} = \Psi_{gr}\cdot(L-1) + L - i - 1$ information packets left, which needs $\Psi_{nd} = (\Psi_{gr}\cdot(L-1) + L - i - 1)\cdot[1/(1-p)]$ NC packets for recovering the lost packets. Therefore, when $L\cdot p > 1$, the service time can be approximately expressed as (13), shown at the bottom of the next page. Finally, the average end-to-end delay of the f-NC HARQ scheme can be calculated by substituting (12) and (13) into (9).

B. Peak AoI

The AoI evolution for a periodical status update in our system is illustrated in Fig. 4, where the HTS generates a status update with a period Δt, A_0 is the initial AoI of the ith status update at UE and we assume that $A_0 = \Delta t$, T_i and T_i' are the time when the ith status update begins and ends, respectively. Then, we have $T_{i+1} - T_i = \Delta t$, and the criteria $T_i' - T_i = \Delta T_i \le \Delta t$ for a successful status updates, where the UE resets AoI as T_1' and T_2' update to A_0 as depicted in Fig. 4. Moreover, if the transmission of the ith status update exceeds Δt, the AoI of T_i' is $2\Delta t$. Then, the HTS would discard the ith status update, and resets AoI to A_0 and clears its buffer,

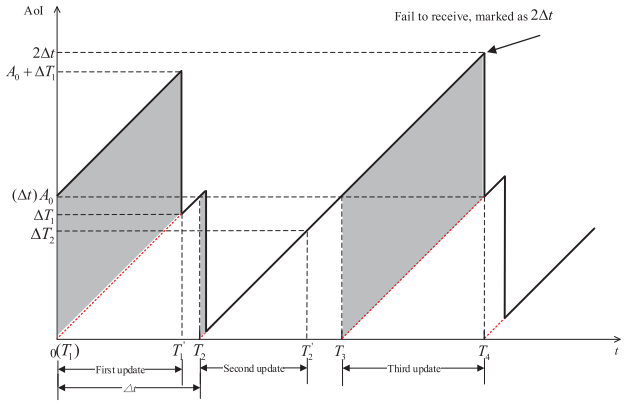

Fig. 4. AoI evolution of a periodical status update system.

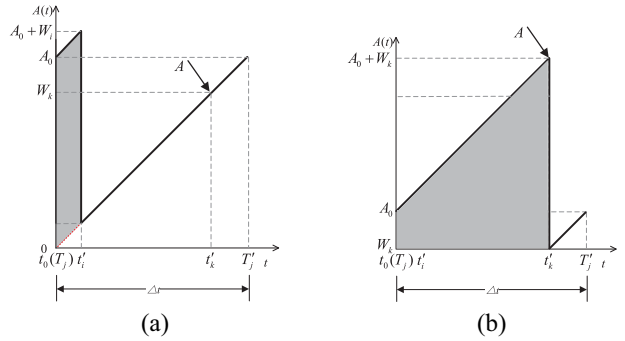

Fig. 5. AoI evolution of a status update transmission. (a) AoI evolution with any information packet has uploaded to the application layer before the last information packet. (b) AoI evolution has backlogged until the last information packet is uploaded to the application layer.

as the AoI of T_4 is A_0 as shown in Fig. 4. Thus, the PAoI $A_i = T_i' - T_i$ is the elapsed time that the ith status update is finally uploaded to the application layer or the end of the ith time interval.

Conclusively, we can focus on the PAoI analysis of a single status update since each status update transmission is independent, and the AoI evolutions of a status update can be divided into two situations as shown in Fig. 5. Without loss of generality, we can define t_i $(i = 1, 2, \ldots, k)$ as the generation time of the information packet d_i, and t_i' as the time when d_i is uploaded to the application layer of UE. Note that the generation time of a status update is the same, and we assume that $t_0 = t_i$. Thus, W_i can be rewritten as $W_i = t_i' - t_0$, and W_k represents the elapsed time of last information packet in this status update, which implies that the PAoI is related to W_k.

As shown in Fig. 5(a), when d_i is successfully received at t_i', the AoI decreases to W_1, and then AoI continues to linearly increase until d_k is uploaded to the application layer. We denote this AoI evolution as Case 1, and the PAoI can be expressed as $A = W_k$. Moreover, if there is no d_i has successfully received before d_k as shown Fig. 5(b), we denote this AoI evolution as Case 2 and the PAoI is $A = A_0 + W_k$. Then, we have

$$A = \begin{cases} W_k, & \text{Case 1} \\ W_k + A_0, & \text{Case 2.} \end{cases} \tag{14}$$

Therefore, the expectation of A can be derived as

$$\begin{aligned} E(A) &= \Pr\{\text{Case 1}\}W_k + \Pr\{\text{Case 2}\}(W_k + A_0) \\ &= W_k + \Pr\{\text{Case 2}\} \cdot A_0. \end{aligned} \tag{15}$$

Note that W_k is correlative to $W_q(k)$ and $W_s(k)$ as shown in (7), which depends on the total number of transmitted packets $\hat{N}$, and W_k can be further expressed as $W_k = t_r + \hat{N} \cdot t_s$. Then, the expectation of $\hat{N}$ can be expressed as follows:

$$\begin{aligned} E\left(\hat{N}\right) = k + \frac{k}{L-1} &\sum_{i=0}^{\lfloor \frac{k(1-p)}{L-1} \rfloor} C_k^i \cdot p^i \cdot (1-p)^{k-i} \\ &+ \sum_{i=\lfloor \frac{k(1-p)}{L-1}+1 \rfloor}^{k} i \cdot C_k^i \cdot p^i \cdot (1-p)^{k-i-1}. \end{aligned} \tag{16}$$

Moreover, the analysis of second part of (15) can also utilize the busy/idle stage, when $L \cdot p < 1$. Thus, the entire transmission process has only one busy stage in Case 2 as shown in Fig. 5(b). Therefore, the probability of Case 2 can be written as

$$\Pr(\text{Case 2}) = \Pr\left(\chi \geq \frac{k}{L-1}\right). \tag{17}$$

When $L \cdot p > 1$, if any information packet of the first group is failed to recover, the remaining Ψ_{gr} groups are backlogged until d_k is recovered. Therefore, the probability of Case 2 can be written as

$$\Pr(\text{Case 2}) = p^L + L \cdot p^{L-1} \cdot (1-p). \tag{18}$$

Finally, by substituting (16), (17), and (18) into (15), the PAoI can be further written as (19), shown at the bottom of the next page.

IV. Optimization of A-NC HARQ

In this section, we design the A-NC HARQ scheme with POMDP and solve it with a lower complexity algorithm. The detailed introduction is as follows.

A. POMDP Formulation

The parameterization of our POMDP problem with feedback delay T and propagation delay t_r can be denoted as $<S, Z, \mathcal{A}, Tr, R, O, \delta, \mathcal{V}>$, and each parameter is introduced in the following.

1) The system state set S, where $s_{t,\iota} = (u, \iota)$ denotes that there are u $(0 \leq u \leq k)$ transmitted information packets, and ι $(0 \leq \iota \leq u)$ lost information packets at t.

$$\lim_{k\to\infty} \frac{1}{k} E\left(\sum_{i=1}^{k} W_s(i)\right) \approx \sum_{l=0}^{\frac{k}{L-1}-1} \sum_{i=1}^{L-1} P_{out} \cdot \left(\frac{\Psi_{tp} \cdot (\Psi_{tp}+1)}{2} - \frac{\Psi_{gr} \cdot \left(\Psi_{gr}-1\right) \cdot L}{2}\right) \cdot \frac{t_s}{k} + \Psi_{ip} \cdot (\Psi_{nd} - \Psi_{tp}) \cdot \frac{t_s}{k} \tag{13}$$

2) The observation set Z, where $z_{t-t_r} = \iota$ indicates that there are ι lost information packets which are observed at the transport layer at $t - T$.
3) The action set of HTS $\mathcal{A}$, where $\mathcal{A} = \{L_1, L_2, \ldots, L_n, \ldots, L_T, L_{T+1}\}$, and $a_t = L_n$ represents HTS selects $L_n = n$ at t, and L_{T+1} means the HTS transmits T information packets until receives z_{t+T-t_r} from the next NAK.
4) *Tr:* $S \times \mathcal{A} \times S \to \Pi(Tr)$ represents the state transition function, where $Tr(s_{t,\iota}, a_t, s_{t+T,\iota'})$ denotes the transition probability distribution from the current state $s_{t,\iota} \in S$ to the next state $s_{t+T,\iota'} \in S$, when the action $a_t \in A$ has been applied.
5) *R:* $S \times \mathcal{A} \to \Pi(R)$ denotes the reward function, where $R(s_{t,\iota}, a_t)$ denotes the immediate reward by taking action a_t under state $s_{t,\iota}$.
6) *O:* $S \times \mathcal{A} \times Z \to \Pi(O)$ is the observation function, where $O(s_{t,\iota}, a_{t-T}, z_{t-t_r})$ represents the probability distribution of observation z_{t-t_r} at HTS, when it reaches $s_{t,\iota}$ under action a_{t-T}.
7) δ: The belief state of system state set S, where $\delta_t(s_{t,\iota})$ denotes the probability of each state $s_{t,\iota}$ in S, and it satisfies $\sum_{s_{t,\iota} \in S} \delta_t(s_{t,\iota}) = 1$.
8) $\mathcal{V}$: The return set with belief state δ and action A, where $v_i^t \in \mathcal{V}$ is the return vector by traversing all possible actions in the $|S|$-dimension belief state δ_t,

Note that we can ignore the subscript t of $s_{t,\iota}$ in POMDP. Moreover, the belief state δ_t depends on the latest observation of z_{t-t_r}, the previous action a_{t-T}, and the previous belief state δ_{t-T}, which can be calculated by Bayes' rule as follows:

$$\begin{aligned}\delta_t(s_\iota) &= \Pr\left(s_\iota \middle| z_{t-t_r}, a_{t-T}, \delta_{t-T}\right) \\ &= \frac{O\left(s_\iota, a_{t-T}, z_{t-t_r}\right) \sum_{s_{\iota'} \in S} Tr(s_{\iota'}, a_{t-T}, s_\iota) \delta_{t-T}(s_{\iota'})}{\sum_{s_\iota \in S} O\left(s_\iota, a_{t-T}, z_{t-t_r}\right) \sum_{s_{\iota'} \in S} Tr(s_{\iota'}, a_{t-T}, s_\iota) \delta_{t-T}(s_{\iota'})}.\end{aligned} \tag{20}$$

The optimal policy for POMDP is choosing the next action to get maximum long-term return. We define V as the value function to represent the return of a_t under δ_t, and V can be expressed as the equivalent Bellman equation

$$V^*(\delta_t) = \max_{a_t \in \mathcal{A}} \sum_{s_\iota \in S} \left\{ \delta_t(s_\iota) R(s_\iota, a_t) + \hat{\gamma} \sum_{z_{t+T-t_r} \in Z} O\left(s_\iota, a_t, z_{t+T-t_r}\right) \times V^*\left(\tau\left(\delta_t, a_t, z_{t+T-t_r}\right)\right) \right\} \tag{21}$$

where $\hat{\gamma} \in [0, 1)$ is the discount factor, which aims to ensure that long-term return converges, $\tau(\delta_t, a_t, z_{t+T-t_r})$ denotes the next belief state δ_{t+T} and $R(s_\iota, a_t)$ is the reward function. The goal of solving POMDP is to find the optimal strategy π^* to maximize the expected cumulative return. Therefore, given the optimal value function V^*, the optimal strategy π^* can be expressed as

$$\pi^*(\delta_t) = \arg\max_{a_t \in \mathcal{A}} \sum_{s_\iota \in S} \left\{ \delta_t(s_\iota) R(s_\iota, a_t) + \hat{\gamma} \sum_{s_{\iota'} \in S} Tr(s_\iota, a_t, s_{\iota'}) \times V^*\left(\tau\left(\delta_t, a_t, z_{t+T-t_r}\right)\right) \right\}. \tag{22}$$

We then define the return vector v_i^t, which can be expressed by the fast informed bound (FIB) as follows [38]:

$$v_i^{t+1}(s_\iota) = \sum_{s_{\iota'} \in S} O\left(s_{\iota'}, a_t, z_{t+T-t_r}\right) \times \sum_{s_\iota \in S} Tr(s_{\iota'}, a_t, s_\iota) \delta_t(s_\iota) v_i^t(s_\iota). \tag{23}$$

Moreover, (21) can be further expressed with v_i^t as [37]

$$V^*(\delta_t) = \max_{a_t \in \mathcal{A}} \sum_{s_\iota \in S} \left\{ \delta_t(s_\iota) R(s_\iota, a_t) + \hat{\gamma} \sum_{z_{t+T-t_r} \in Z} \left(\max_{v_i^t \in \mathcal{V}} \Xi(\delta_t, v_i(s_\iota)) \right) \right\} \tag{24}$$

where $\Xi(\cdot, \cdot)$ is the inner product.

B. A-NC HARQ Scheme Optimization

In this section, we analyze the A-NC HARQ scheme with $T = 3$ and $t_r = 1$ in Fig. 2(b) to achieve the lowest the average end-to-end delay and PAoI. Moreover, we assume that the action set is $A = [L_b, L_T, L_g]$, where $L_b = L_1 = 1$ means HTS only transmits NC packets, $L_T = 3$, and $L_g = L_{T+1} = 4$ means HTS only transmits information packets in the next T time slot until the HTS receives z_{t+2} from the next NAK to adjust L. Moreover, the HTS will switch to L_b when $i = k$ and it does not receive an ACK. Therefore, the observation function with s_ι, z_t and $a_{t-T} = L_T$ can be written as

$$O\left(s_\iota, L_T, z_{t-t_r}\right) = \begin{cases} p^3, & \text{if } z_{t-t_r} = 2 \\ C_3^2 \cdot p^2 \cdot (1-p), & \text{if } z_{t-t_r} = 1 \\ C_3^1 \cdot p \cdot (1-p)^2, & \text{if } z_{t-t_r} = 0 \\ (1-p)^3, & \text{if } z_{t-t_r} = -1 \\ 0, & \text{otherwise} \end{cases} \tag{25}$$

where p is BLER.

$$E(A) = t_r + \Pr\left(\text{Case } 2\right) \cdot A_0 + t_s \left(k + \frac{k}{L-1} \sum_{i=0}^{\lfloor \frac{k(1-p)}{L-1} \rfloor} C_k^i \cdot p^i \cdot (1-p)^{k-i} + \sum_{i=\lfloor \frac{k(1-p)}{L-1} + 1 \rfloor}^{k} C_k^i i \cdot p^i \cdot (1-p)^{k-i-1} \right) \tag{19}$$

Algorithm 1: A-NC HARQ Transmission Scheme for POMDP

Input: δ, $\bar{V}$, Z, S,p, T, k, π,
Output: The optimal action set of transmission
Initialize $\mathcal{A}$ = [1,1.5,3,4], $n_p = 0$,$n = T$+1;
Initialize $N_{tr} = [-3, -1, 1, 3]$, $N_d = [0, 1, 2, 3]$;
for $i = 1; i \le n; i++$ **do**
  $a_i = \mathcal{A}[\lfloor n_p \times p \rfloor]$, $\pi = [\pi\ a_i]$,
  $n_p = n_p + N_{tr}[\lceil a_i \rceil]$, update ι.
end
while $u \le k$ **do**
  a_i = iFIB(π, u,p, ι,T), update π, ι, i, u.
end
return π

Then, the transition function with s_ι, $s_{\iota'}$ and $a_{t-T} = L_T$ can be written as

$$Tr(s_\iota, L_T, s_{\iota'}) = \begin{cases} p^3, & \text{if } \iota' = \iota + 2 \\ C_3^2 \cdot p^2 \cdot (1-p), & \text{if } \iota' = \iota + 1 \\ (1-p)^3(1 - \mathbb{1}(\iota \ge 1)) & \\ + C_3^1 \cdot p \cdot (1-p)^2, & \text{if } \iota' = \iota \\ (1-p)^3 \mathbb{1}(\iota \ge 1), & \text{if } \iota' = \iota - 1 \\ 0, & \text{otherwise} \end{cases} \tag{26}$$

where $\mathbb{1}(\cdot)$ represent the indicator function.

Furthermore, in the A-NC HARQ scheme, we can adjust L to reduce the queue length at the transport layer in every T. Therefore, we infer that reward function $R(s_\iota, a_t)$ is related to ι. In addition, we define $\mathbf{X}$ as the probability distribution of how many packets were lost during T, and $\mathbf{I}$ as the results when a_t is applied. For example, when $a_t = L_T = 3$, $\mathbf{X} = [(1-p)^3, 3p(1-p)^2, 3p^2(1-p), p^3]$, and $\mathbf{I} = [-1, 0, 1, 2]$. Therefore, $R(s_\iota, a_t)$ can be expressed as $R(s_\iota, a_t) = -\iota - \Xi(\mathbf{X}, \mathbf{I})$. Moreover, $v_i^t(s_\iota)$ is upper bounded as follows:

$$v_i^t(s_\iota) \le -\frac{(k-u+\iota)\cdot(\iota-1)}{1-p} - \frac{(k-u+1)\cdot(k-u)}{2\cdot(1-p)}. \tag{27}$$

Thus, the upper bound of value function $\bar{V}(\delta)$ can be found by taking (27) into (24).

In addition, when the HTS cannot receive feedback, i.e., $T \to \infty$, the decision of HTS is completely based on prediction. Therefore, to address the intractable value iterations in POMDP with a conventional value iteration algorithm, we utilize the upper bound $\bar{V}(\delta)$ to design an iFIB algorithm and solve the POMDP problem in our A-NC HARQ scheme.

C. iFIB Algorithm and Complexity Analysis

Our iFIB has a low computational complexity due to the tight upper bound (26), and it proceeds via traversing all possible actions a^* to maximize the upper bound $\bar{V}(\delta)$. The HTS starts with an initial L at first when it does not receive NAK, and then it updates brief status when it receives delayed feedback NAK. Algorithms 1 and 2 summarize the process of the iFIB algorithm in detail.

Algorithm 2: Function a_i = iFIB(π, u, p, ι,T)

Input: π,u, p, ι,T
Output: The optimal policy for the current step
calculate s and δ with u, ι;
Initialize $\bar{V} = [v_1, v_2, v_3, v_4]$;
for *all* $a_i \in \mathcal{A}$ **do**
  for *all* $z_j \in Z$ **do**
    update δ' with (z_j, a, δ), and calculate the reward $v_{i,j}$ of the action a_i at observation z_j with δ';
  end
  calculate the reward v_i of the action a_i with $v_i = \sum_{z_j \in Z} O(s, a, z_j) \cdot v_{i,j}$
end
$a_i = \arg\max_{a_i \in \mathcal{A}} \bar{V}$.
return a_i.

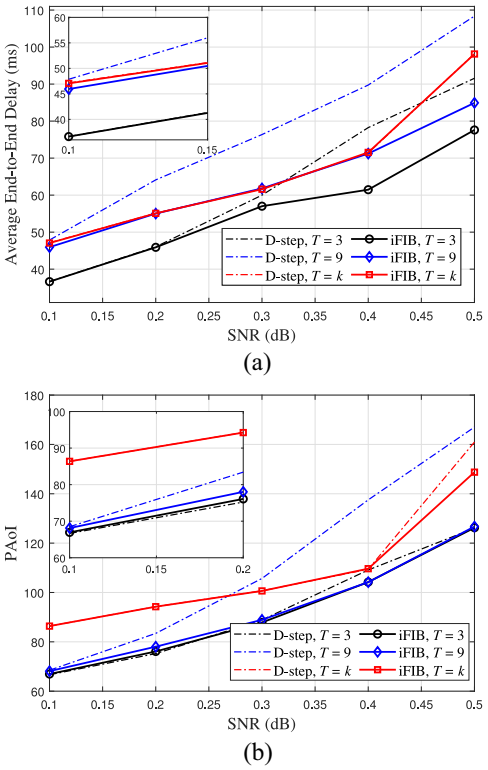

Fig. 6. Performance of the A-NC HARQ scheme by optimizing via iFIB and D-step search algorithm. (a) Average end-to-end delay versus BLER. (b) PAoI versus BLER.

Moreover, we simulate the average end-to-end delay and PAoI of the A-NC HARQ scheme by optimizing via iFIB with different T, and compare with the D-step search algorithm [15] as shown in Fig. 6(a) and (b). We can observe that the average end-to-end delay and PAoI of POMDP solved by two algorithms are similar. Note that the total number of states in POMDP is $O(|S|) = O(k^2)$, the total number of observations is $O(|Z|) = O(T)$, and the total number of actions is $O(|\mathcal{A}|) = O(T)$. Since δ is limited by S, the maximum number of greedy search is $O(k^2)$. In addition, the complexity in Algorithm 2 is $O(T)$. Therefore, the complexity of the

TABLE II
SIMULATION PARAMETERS

Parameters	Value
Average power of scatter component b_0	0.063
Average power of LoS component Ω	0.00897
Nakagami-m parameter m	1
Packet size B	$[200, 500, 1000]$ bits
Status update size k	[60, 100]
Code intervals L	$[2, 3, 5, 11]$
Feedback delay T	$[1, 5, \infty]$
Status update interval Δt	350 ms
Initial AoI A_0	350 ms
Time slot t	1 ms
Propagation delay t_r	1 ms
Transmission delay t_s	1 ms

TABLE III
SHADOWED-RICIAN FADING PARAMETERS

Shadowing	b_i	Ω_i	m_i
Infrequent light shadowing (ILS)	0.158	1.29	20
Average shadowing (AS)	0.126	0.835	11
Frequent heavy shadowing (FHS)	0.063	0.000897	1

iFIB algorithm is $O(T^2 \cdot k^4)$. On the other hand, the D-step search algorithm constructs the next reachable beliefs under the selected leaf for some predetermined expansion depth D and evaluates the approximate value function for all newly created nodes. Thus, the complexity of the D-step search algorithm is $O(T^{2D} \cdot k^6)$ [39].

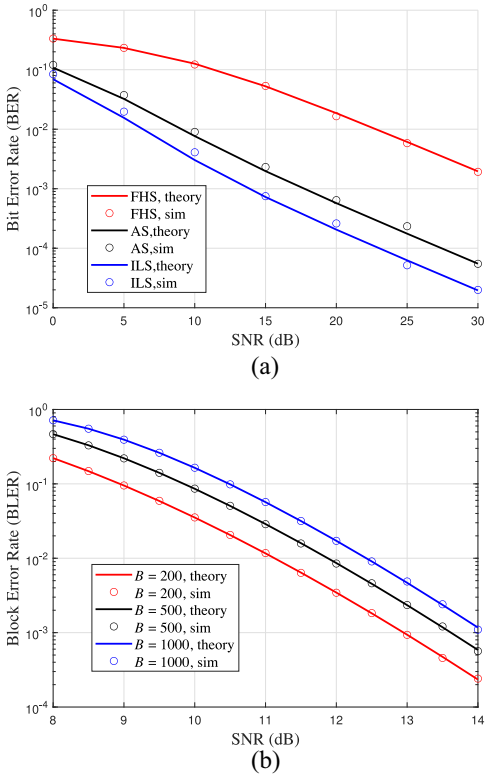

Fig. 7. BER versus SNR under FHS, ILS, and AS SR fading parameters, and the BLER performance for $N = 8$ under different packet size. (a) BER performance. (b) BLER performance.

V. SIMULATION RESULTS AND DISCUSSION

In this section, we present the simulation results to validate the accuracy of our derivation and evaluate the performance of our proposed f-NC HARQ and A-NC HARQ schemes, and the simulation parameters are given in Table II. Moreover, the fading parameters of infrequent light shadowing (ILS), average shadowing (AS), and frequent heavy shadowing (FHS) are summarized in Table III.

The BER performance under FHS, ILS, and AS SR fading parameters are shown in Fig. 7(a), and validate the accuracy of our derivation. Moreover, note that Fig. 3 shows that the reliable transmission over SR channel with FHS needs multiple antennas. Then, we simulate the BLER performance with $N = 8$ and $B = 200, 500, 1000$ bits as shown in Fig. 7(b). Simulation results validate our derivation of BLER and show that $N = 8$ antennas can ensure the reliable transmission over SR channel with FHS. Note that the BLER increases with the packet size, because we do not utilize physical layer coding schemes in our NC HARQ scheme yet. Consider that the limited number of finite block-length packets in each status update in our NC HARQ scheme, if we utilize advance physical layer coding, such as 5G NR LDPC codes, 5G NR Polar codes, and TBCC [31] to combine with HARQ [40], [41], the BLER performance of our NC HARQ can be significantly decreased. However, the finite block-length capacity over the SR channel is still missing, and the cross-layer error control transmission scheme is left as a future challenge. Thus, we utilize FHS and $N = 8$, $B = 1000$ bits in the following simulations.

We first simulate the f-NC HARQ scheme with $L = 2, 3$ to validate the accuracy of our derivations as shown in Fig. 8. It can be observed that the theoretical derivations of average end-to-end delay in (9), the average number of transmitted packets in (15), and PAoI in (18) are agreed well with the simulation results in Fig. 8(a)–(c), respectively. Moreover, all the three performance parameters fall to the floor region with $L = 2$ at SNR $\geq$ 9 dB, and with $L = 3$ at SNR $\geq$ 10 dB, which indicates that there is an optimal L in different SNR regions. When L is not small enough to provide sufficient NC packets during the status updates in the low SNR region, the lost information cannot be recovered and retransmission is needed in the f-NC HARQ scheme, as these three performance parameters are significant high in SRN $\in \{8, 10\}$ dB region. This also motivated us to design the A-NC HARQ scheme to adapt L during the status update transmissions to avoid the retransmission.

Moreover, we present the average end-to-end delay and PAoI of the f-NC HARQ scheme and compare with the conventional NC HARQ with code rate $R = (1/2)$ in Fig. 9. The NC packet in the conventional NC HARQ scheme is transmitted after all the information packets have been transmitted. As shown in Fig. 9(a) and (b), we can observe that the f-NC HARQ scheme can achieve lower average end-to-end delay and PAoI than the conventional NC HARQ scheme with $L = 2$ when SNR $\geq$ 9 dB. The main reason is that the NC packets are inserted into information packets in the f-NC HARQ scheme, which can accelerate the recovery of

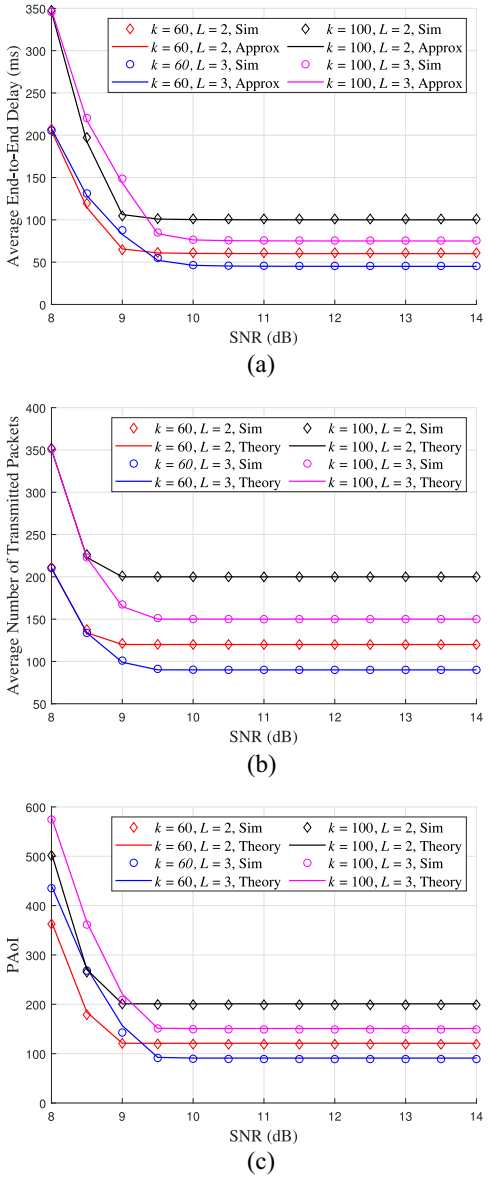

Fig. 8. Performance of f-NC HARQ with different k. (a) Average end-to-end delay versus SNR. (b) Average number of transmitted packets versus SNR. (c) PAoI versus SNR.

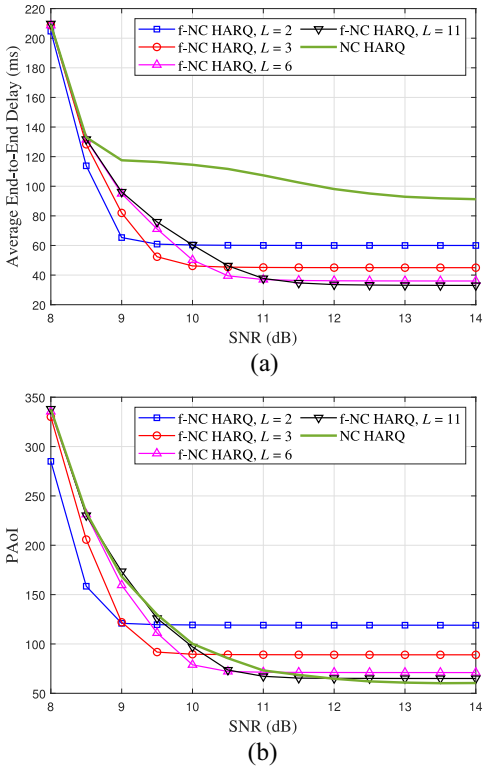

Fig. 9. Comparison of f-NC HARQ and conventional NC HARQ scheme, the number of information packets is $k = 60$. (a) Average end-to-end delay versus SNR. (b) PAoI versus SNR.

the lost information packets and lower the average end-to-end delay and PAoI than the conventional NC HARQ scheme. Furthermore, when SNR $\geq$ 13 dB, the PAoI of the NC HARQ scheme gradually lowers than the f-NC HARQ with different L as shown in Fig. 9(b). Because the NC HARQ transmits information packets in the first k positions and followed k NC packets, and the UE needs less NC packets to recover lost information packets and upload the status update to the application layer in the high SNR region, thus leads to lower PAoI than the f-NC HARQ scheme.

The A-NC HARQ scheme has lower average end-to-end delay and PAoI compare to the f-NC HARQ scheme as shown in Fig. 10(a) and (b). The main reason is the f-NC HARQ scheme with fixed L is not applicable in S-IoT due to the very marked variations over SR fading channel, and the A-NC HARQ scheme can utilize the delayed feedback NAK to reselect an appropriate L to adjust the number of NC packets. Furthermore, when SNR $\geq$ 13 dB, the average end-to-end delay and PAoI of the f-NC HARQ scheme with L is limited to $t_r+([(k-1)L-1]/[2(L-1)])\cdot t_s$ and $t_r+(k+[k/(L-1)])\cdot t_s$, respectively, while that of the A-NC HARQ scheme approach $t_r+[(k-1)/2]\cdot t_s$ and $t_r+k\cdot t_s$, respectively. Moreover, we can observe that the NC HARQ gradually approaches the A-NC HARQ, which validates the effectiveness of our design.

Finally, note that the A-NC HARQ scheme has lower average end-to-end delay and PAoI than that of the f-NC HARQ scheme in high SNR region, which depends on the number of NC packets. Therefore, we can calculate the throughput as follows:

$$\varsigma = \frac{\text{Number of information packets}}{\text{Number of transmitted packets}} = \frac{k}{E(\hat{N})}. \quad (28)$$

The performance comparison of throughput in these two schemes versus SNR is shown in Fig. 10(c). We can observe that when the SNR $\in \{8, 9\}$ dB, the throughput of two schemes is closed. When SNR $\geq$ 9 dB, the A-NC HARQ scheme can achieve higher throughput. The main reason is when SNR is low, the A-NC HARQ scheme will select small L to ensure the transmission reliability, and reselect larger L with the increase of SNR in each T time slot.

VI. Conclusion

In this article, we modeled an end-to-end transmission in the S-IoT scenario, in which an LEO HTS collects a status update with multiple packets and transmitted them to the

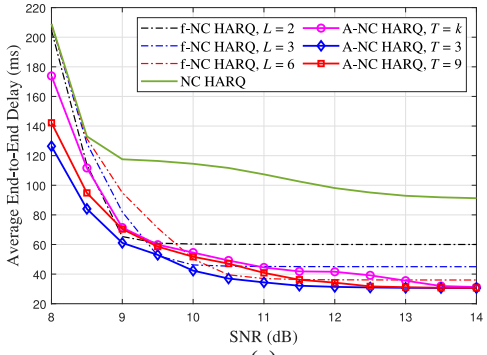

(a)

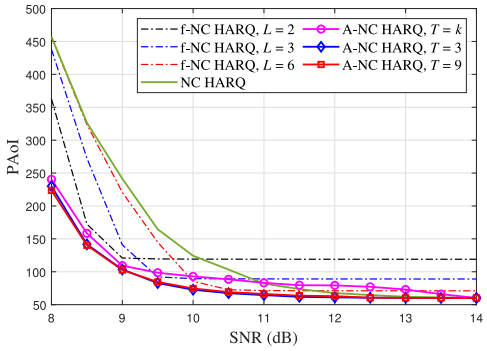

(b)

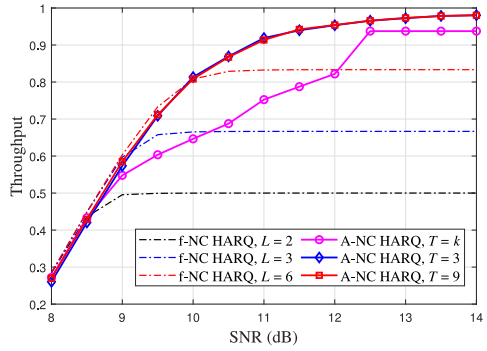

(c)

Fig. 10. Comparison of A-NC HARQ and f-NC HARQ scheme, the number of information packets is $k = 60$. (a) Average end-to-end delay versus SNR. (b) PAoI versus SNR. (c) Throughput versus SNR.

UE, and these packets need to be decoded successfully at the transport layer of UE before being uploaded to the application layer. We derived the closed-form expression of BER over SR fading channel with single antenna and with MIMO system, respectively, and further utilized the theoretical derivations to predetermine an appropriate L for guaranteeing the timely status update in the f-NC HARQ and A-NC HARQ schemes. Moreover, to further decrease the average end-to-end delay and PAoI, we optimized the A-NC HARQ scheme based on POMDP and solved it via a lower complexity iFIB algorithm. Simulation results validate the accuracy of our derivation of BER, average end-to-end delay, and PAoI and show that the A-NC HARQ scheme can achieve the lowest PAoI and average end-to-end delay. There are several possible avenues in future research, which includes taking energy overhead into consideration to achieve the maximum energy efficiency, as well as considering continuous status update with multiple packets.

APPENDIX A
DERIVATION OF BER EXPRESSION IN SR FADING CHANNEL

First, we derive the BER expression (2) of the SR fading channel, and the BER of M-PSK with instant SNR r can be expressed as follows [11]:

$$P_e(r) = \frac{2}{\zeta_M} \sum_{j=1}^{\max(M/4,1)} Q\left(\sqrt{2r}b_k\right) \tag{29}$$

where $\zeta_M = \max(\log_2 M, 2)$ and $b_k = \sin([(2k-1)\pi]/M)$.

Then, based on the PDF of SR fading distribution in (2) and the BER of M-PSK in (29), the BER of the SR fading channel can be derived through calculate $P_e = \int f(r)P_e(r)dr$, and we have

$$\begin{aligned} P_e &= \int f(r)P_e(r)dr \\ &= \int \frac{2}{\zeta_M} \sum_{j=1}^{\max(M/4,1)} Q\left(\sqrt{2r}b_k\right) \cdot \frac{1}{2b_0\gamma}\left(\frac{2b_0 m}{2b_0 m+\Omega}\right)^m \\ &\quad \cdot \exp\left(-\frac{r}{2b_0\gamma}\right) \cdot {}_1F_1\left(m, 1, \frac{1}{2b_0\gamma}\left(\frac{\Omega}{(2b_0 m+\Omega)}\right)r\right)dr \end{aligned} \tag{30}$$

where

$$\begin{aligned} &{}_1F_1\left(m; 1; \frac{1}{2b_0\gamma}\left(\frac{\Omega}{(2b_0 m+\Omega)}\right)r\right) \\ &= \exp\left(\frac{1}{2b_0\gamma}\left(\frac{\Omega}{(2b_0 m+\Omega)}\right)r\right) \\ &\quad \times \sum_{1}^{m-1} \frac{(-1)^k(1-m)_k\left(\frac{1}{2b_0\gamma}\left(\frac{\Omega}{(2b_0 m+\Omega)}\right)r\right)^k}{(k!)^2}. \end{aligned} \tag{31}$$

Therefore, we have

$$\begin{aligned} P_e &= \int f(r)P_e(r)dr \\ &= \int_0^\infty \sum_{k=0}^{m-1} \alpha e^{-\eta r}\theta_k \frac{r^k}{k!} \\ &\quad \times \int_{\sqrt{2\gamma}b_j}^\infty \frac{2}{\zeta_M} \sum_{j=1}^{\max(M/4,1)} \frac{1}{\sqrt{2\pi}} e^{-\frac{t^2}{2}} dtdr \\ &= \int_0^\infty \frac{2}{\zeta_M} \sum_{j=1}^{\max(M/4,1)} \frac{1}{\sqrt{2\pi}} e^{-\frac{t^2}{2}} \\ &\quad \times \int_0^{\frac{t^2}{2b_j^2}} \sum_{k=0}^{m-1} \alpha e^{-\eta r}\theta_k \frac{r^k}{k!} drdt \end{aligned} \tag{32}$$

where $\theta_k = ([(-1)^k(1-m)_k]/k!)([1/(2b_0\gamma)][\Omega/(2b_0 m + \Omega)])^k$. Thus, we can finally get the derivation of BER in SR

fading channel as follows:

$$P_e = \int_0^{\infty} \frac{2}{\zeta_M} \sum_{j=1}^{\max(M/4,1)} \frac{1}{\sqrt{2\pi}} e^{-\frac{t^2}{2}} \sum_{k=0}^{m-1} \alpha\theta_k \times \left(\frac{1}{\eta^{k+1}} - e^{-\frac{\eta t^2}{2b_j^2}} \sum_{i=0}^{k} \frac{1}{i!} \frac{t^{2i}}{2^i b_j^{2i} \eta^{k-i+1}} \right) dt = \sum_{k=0}^{m-1} \alpha\theta_k \sum_{j=1}^{\max(M/4,1)} \frac{1}{\zeta_M} \times \left(\frac{1}{\eta^{k+1}} - \frac{1}{\sqrt{2\pi}} \sum_{i=0}^{k} \frac{1}{i!} \frac{1}{2^{i-v} b_j^{2i} \eta^{k-i+1} \left(1+\eta/b_j^2\right)^v} \Gamma(v) \right] \tag{33}$$

where $\alpha = [1/(2b_0\gamma)([2b_0m]/[2b_0m + \Omega])^m$, $\eta = (m/[(2b_0m + \Omega)\gamma])$, $v = [(2i + 1)/2]$, and Γ is the Gamma function.

APPENDIX B
DERIVATION OF BER EXPRESSION WITH MIMO IN CLOSED FORM

The BER with MIMO in SR fading channel can be rewritten as

$$P_e(\gamma) = \int f_Z(r) P_e(r) dr \tag{34}$$

where $P_e(r)$ is the BER of M-PSK in AWGN channel, and $f_Z(r)$ is the PDF of instantaneous SNR of SR fading channel with MIMO. Moreover, the sum of N independent random variables can be viewed as a convolution of these random variables, and we set $m = 1$ to simplify (2). Therefore, (2) can be rewritten as

$$f(r) = \alpha e^{-\eta r} \tag{35}$$

where $\alpha = [1/(2b_0\gamma)]([2b_0m]/[2b_0m + \Omega])^m$ and $\eta = (m/[(2b_0m+\Omega)\gamma])$. Equation (35) can be viewed as a negative exponential distribution, and the convolution of N negative exponential distributions can be expressed as an Erlang distribution [42], which can be expressed as

$$f_Z(r) = \frac{\alpha^N}{(N-1)!} r^{N-1} e^{-\eta r}. \tag{36}$$

Therefore, (34) can be rewritten as

$$P_e(\gamma) = \int_0^{\infty} \frac{\alpha^N}{(N-1)!} r^{N-1} e^{-\eta r} \times \int_{\sqrt{2}rb_j}^{\infty} \frac{2}{\zeta_M} \sum_{j=1}^{\max(M/4,1)} \frac{1}{\sqrt{2\pi}} e^{-\frac{t^2}{2}} dt dr = \int_0^{\infty} \frac{2}{\zeta_M} \sum_{j=1}^{\max(M/4,1)} \frac{1}{\sqrt{2\pi}} e^{-\frac{t^2}{2}} \times \int_0^{\frac{t^2}{2b_j}} \frac{\alpha^N}{(N-1)!} r^{N-1} e^{-\eta r} dr dt. \tag{37}$$

Conclusively, we can get the closed-form expression by integrate (37) as follows:

$$P_e(\gamma) = \int_0^{\infty} \frac{2}{\zeta_M} \sum_{j=1}^{\max(M/4,1)} \frac{1}{\sqrt{2\pi}} e^{-\frac{t^2}{2}} \times \alpha^N \left(\frac{1}{\eta^N} - e^{-\frac{\eta t^2}{2b_j^2}} \sum_{i=0}^{N-1} \frac{1}{i!} \frac{t^{2i}}{2^i b_j^{2i} \eta^{N-i}} \right) dt = \alpha^N \sum_{j=1}^{\max(M/4,1)} \frac{1}{\zeta_M} \times \left[\frac{1}{\eta^N} - \frac{1}{\sqrt{2\pi}} \sum_{i=0}^{N-1} \frac{1}{i!} \frac{1}{2^{i-v} b_j^{2i} \eta^{N-i} \left(1+\eta/b_j^2\right)^v} \Gamma(v) \right]. \tag{38}$$

REFERENCES

[1] M. Centenaro, C. E. Costa, F. Granelli, C. Sacchi, and L. Vangelista, "A survey on technologies, standards and open challenges in satellite IoT," *IEEE Commun. Surveys Tuts.*, vol. 23, no. 3, pp. 1693–1720, 3rd Quart., 2021.

[2] J. Jiao, S. Wu, R. Lu, and Q. Zhang, "Massive access in the space-based Internet of Things: Challenges, opportunities, and future directions," *IEEE Wireless Commun.*, vol. 28, no. 5, pp. 118–125, Oct. 2021.

[3] Z. Lin, M. Lin, W.-P. Zhu, J.-B. Wang, and J. Cheng, "Robust secure beamforming for wireless powered cognitive satellite–terrestrial networks," *IEEE Trans. Cogn. Commun. Netw.*, vol. 7, no. 2, pp. 567–580, Jun. 2021.

[4] J. Jiao, Y. He, S. Wu, and Q. Zhang, "Intelligent hybrid nonorthogonal multiple access relaying for vehicular networks in 6G," *IEEE Internet Things J.*, vol. 8, no. 19, pp. 14773–14786, Oct. 2021.

[5] A. Kosta, N. Pappas, and V. Angelakis, *Age of Information: A New Concept, Metric, and Tool*, Now Found. Trends, Hanover, MA, USA, 2017.

[6] S. Kaul, R. Yates, and M. Gruteser, "Real-time status: How often should one update?" in *Proc. IEEE INFOCOM*, 2012, pp. 2731–2735.

[7] J. Jiao, Z. Ni, S. Wu, Y. Wang, and Q. Zhang, "Energy efficient network coding HARQ transmission scheme for S-IoT," *IEEE Trans. Green Commun. Netw.*, vol. 5, no. 1, pp. 308–321, Mar. 2021.

[8] A. Abdi, W. C. Lau, M. Alouini, and M. Kaveh, "A new simple model for land mobile satellite channels: First- and second-order statistics," *IEEE Trans. Wireless Commun.*, vol. 2, no. 3, pp. 519–528, May 2003.

[9] K. An *et al.*, "Performance analysis of multi-antenna hybrid satellite–terrestrial relay networks in the presence of interference," *IEEE Trans. Commun.*, vol. 63, no. 11, pp. 4390–4404, Nov. 2015.

[10] J. Jiao, J. Zhou, S. Wu, and Q. Zhang, "Superimposed pilot code-domain NOMA scheme for satellite-based Internet of Things," *IEEE Syst. J.*, vol. 15, no. 2, pp. 2732–2743, Jun. 2021.

[11] M. R. Bhatnagar and M. K. Arti, "On the closed-form performance analysis of maximal ratio combining in Shadowed-Rician fading LMS channels," *IEEE Commun. Let.*, vol. 18, no. 1, pp. 54–57, Jan. 2014.

[12] M. K. Arti, "Data detection in large MIMO satellite communication systems," *IEEE Wireless Commun. Lett.*, vol. 10, no. 5, pp. 1032–1035, May 2021.

[13] L. Shi *et al.*, "Integration of Reed-Solomon codes to licklider transmission protocol (LTP) for space DTN," *IEEE Aerosp. Electron. Syst. Mag.*, vol. 32, no. 4, pp. 48–55, Apr. 2017.

[14] "Erasure correcting codes for use in near-earth and deep-space communications," Nat. Aeronaut. Space Admin., Washington, DC, USA, document CCSDS 131.5-O-1, 2014. [Online]. Available: https://public.ccsds.org/Pubs/131x5o1.pdf

[15] X. Xu, Y. Zeng, Y. Li, and B. Vucetic, "Minimum-latency FEC design with delayed feedback: Mathematical modeling and efficient algorithms," *IEEE Trans. Wireless Commun.*, vol. 19, no. 11, pp. 7210–7223, Nov. 2020.

[16] M. Karzand, D. J. Leith, J. Cloud, and M. Médard, "Design of FEC for low delay in 5G," *IEEE J. Sel. Areas Commun.*, vol. 35, no. 8, pp. 1783–1793, Aug. 2017.

[17] M. Muhammad, G. Giambene, and T. de Cola, "QoS support in SGD-based high throughput satellite networks," *IEEE Trans. Wireless Commun.*, vol. 15, no. 12, pp. 8477–8491, Dec. 2016.

[18] S. A. M. Ghanem, A. E. Gharsellaoui, D. Tarchi, and A. Vanelli-Coralli, "Network coding channel virtualization schemes for satellite multicast communications," in *Proc. IEEE Global Commun. Conf. (GLOBECOM)*, 2017, pp. 1–6.

[19] S. Liu, J. Jiao, Z. Ni, S. Wu, and Q. Zhang, "Age-optimal NC-HARQ protocol for multi-hop satellite-based Internet of Things," in *Proc. IEEE Wireless Commun. Netw. Conf. (WCNC)*, 2021, pp. 1–6.

[20] S. Kaul, M. Gruteser, V. Rai, and J. Kenney, "Minimizing age of information in vehicular networks," in *Proc. 8th Annu. IEEE Commun. Soc. Conf. Sens. Mesh Ad Hoc Commun. Netw.*, 2011, pp. 350–358.

[21] M. A. Abd-Elmagid, N. Pappas, and H. S. Dhillon, "On the role of age of information in the Internet of Things," *IEEE Commun. Mag.*, vol. 57, no. 12, pp. 72–77, Dec. 2019.

[22] R. Talak and E. Modiano, "Age-delay tradeoffs in single server systems," in *Proc. IEEE Int. Symp. Inf. Theory (ISIT)*, 2019, pp. 340–344.

[23] R. Talak and E. H. Modiano, "Age-delay tradeoffs in queueing systems," *IEEE Trans. Inf. Theory*, vol. 67, no. 3, pp. 1743–1758, Mar. 2021.

[24] M. Costa, M. Codreanu, and A. Ephremides, "Age of information with packet management," in *Proc. IEEE Int. Symp. Inf. Theory (ISIT)*, 2014, pp. 1583–1587.

[25] N. Akar and O. Dogan, "Discrete-time queueing model of age of information with multiple information sources," *IEEE Internet Things J.*, vol. 8, no. 19, pp. 14531–14542, Oct. 2021.

[26] F. Chiariotti, O. Vikhrova, B. Soret, and P. Popovski, "Peak age of information distribution for edge computing with wireless links," Apr. 2020, *arXiv:2004.05088*.

[27] J. Li, Y. Zhou, and H. Chen, "Age of information for multicast transmission with fixed and random deadlines in IoT systems," *IEEE Internet Things J.*, vol. 7, no. 9, pp. 8178–8191, Sep. 2020.

[28] L. You, K.-X. Li, J. Wang, X. Gao, X.-G. Xia, and B. Ottersten, "Massive MIMO transmission for LEO satellite communications," *IEEE J. Sel. Areas Commun.*, vol. 38, no. 8, pp. 1851–1865, Aug. 2020.

[29] L. You, X. Gao, A. L. Swindlehurst, and W. Zhong, "Channel acquisition for massive MIMO-OFDM with adjustable phase shift pilots," *IEEE Trans. Signal Process.*, vol. 64, no. 6, pp. 1461–1476, Mar. 2016.

[30] D. Goto, H. Shibayama, F. Yamashita, and T. Yamazato, "LEO-MIMO satellite systems for high capacity transmission," in *Proc. IEEE Global Communi. Conf. (GLOBECOM)*, 2018, pp. 1–6.

[31] F. Wang, J. Jiao, K. Zhang, S. Wu, Y. Li, and Q. Zhang, "Self-adaptive ordered statistics decoder for finite block length raptor codes towards URLLC," *IEEE Internet Things J.*, vol. 9, no. 5, pp. 3282–3297, Mar. 2022.

[32] K. Zhang, J. Jiao, Z. Huang, S. Wu, and Q. Zhang, "Finite block-length analog fountain codes for ultra-reliable low latency communications," *IEEE Trans. Commun.*, vol. 68, no. 3, pp. 1391–1404, Mar. 2020.

[33] "CCSDS file delivery protocol (CFDP)—Part 1: Introduction and overview," Nat. Aeronaut. Space Admin., Washington, DC, USA, document CCSDS 720.1-G-4, 2021. [Online]. Available: https://public.ccsds.org/Pubs/720x1g4.pdf

[34] J. Lu, K. B. Letaief, J. C.-I. Chuang, and M. L. Liou, "M-PSK and M-QAM BER computation using signal-space concepts," *IEEE Trans. Commun.*, vol. 47, no. 2, pp. 181–184, Feb. 1999.

[35] M. K. Arti and S. K. Jindal, "OSTBC transmission in Shadowed-Rician land mobile satellite links," *IEEE Trans. Veh. Technol.*, vol. 65, no. 7, pp. 5771–5777, Jul. 2016.

[36] F. P. Fontan, M. Vazquez-Castro, C. E. Cabado, J. P. Garcia, and E. Kubista, "Statistical modeling of the LMS channel," *IEEE Trans. Veh. Technol.*, vol. 50, no. 6, pp. 1549–1567, Nov. 2001.

[37] E. J. Sondik, "The optimal control of partially observable Markov processes over the infinite horizon: Discounted costs," *Oper. Res.*, vol. 26, no. 2, pp. 282–304, 1978. [Online]. Available: https://www.jstor.org/stable/169635

[38] M. Hauskrecht, "Incremental methods for computing bounds in partially observable Markov decision processes," in *Proc. 14th Nat. Conf. Artif. Intell.*, 1997, pp. 734–739.

[39] S. Ross, J. Pineau, S. Paquet, and B. Chaib-draa, "Online planning algorithms for POMDPs," *J. Artif. Intell. Res.*, vol. 32, pp. 663–704, Aug. 2008.

[40] B. Makki, T. Svensson, and M. Zorzi, "Finite block-length analysis of the incremental redundancy HARQ," *IEEE Wireless Commun. Lett.*, vol. 3, no. 5, pp. 529–532, Oct. 2014.

[41] F. Nadeem, M. Shirvanimoghaddam, Y. Li, and B. Vucetic, "Non-orthogonal HARQ for delay sensitive applications," in *Proc. IEEE Int. Conf. Commun. (ICC)*, 2020, pp. 1–6.

[42] R. W. Wolf, *Stochastic Modeling and the Theory of Queues*. Englewood Cliffs, NJ, USA: Prentice Hall, 1989.

Jing Ding received the B.S. degree in communication engineering from Zhengzhou University, Zhengzhou, China, in 2020. He is currently pursuing the M.S. degree with Harbin Institute of Technology (Shenzhen), Shenzhen, China.

His current research interests include satellite-based Internet of Things, HARQ, and age of information.

Jian Jiao (Member, IEEE) received the M.S. and Ph.D. degrees in communication engineering from Harbin Institute of Technology, Harbin, China, in 2007 and 2011, respectively.

From 2011 to 2015, he was a Postdoctoral Research Fellow with the Communication Engineering Research Centre, Shenzhen Graduate School, Harbin Institute of Technology Shenzhen (HITsz), Shenzhen, China. From 2016 to 2017, he was a China Scholarship Council Visiting Scholar with the School of Electrical and Information Engineering, The University of Sydney, Sydney, NSW, Australia. From 2017 to 2019, he was an Assistant Professor with HITsz, where he has been an Associate Professor with the Department of Electrical and Information Engineering since 2020. He is also an Associate Professor with Peng Cheng Laboratory, Shenzhen. His current interests include error control codes, space communications and networking, and massive random access.

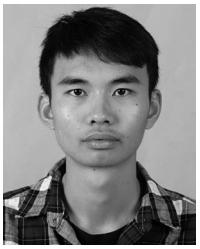

Jianhao Huang received the B.S. degree in communication engineering from Harbin Institute of Technology (Shenzhen), Shenzhen, China, in 2022, where he is currently pursuing the M.S. degree.

His current research interests include satellite communications and age of information.

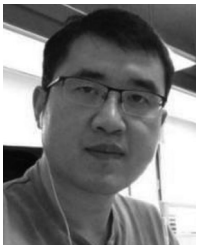

Shaohua Wu (Member, IEEE) received the Ph.D. degree in communication engineering from Harbin Institute of Technology, Harbin, China, in 2009.

From 2009 to 2011, he held a postdoctoral position with the Department of Electronics and Information Engineering, Shenzhen Graduate School, Harbin Institute of Technology (Shenzhen), Shenzhen, China, where he was an Associate Professor from 2012 to 2020. Since 2021, he has been a Professor with the School of Electrical and Information Engineering, Harbin Institute of Technology (Shenzhen), and also a Professor with Peng Cheng Laboratory, Shenzhen. His current research interests include wireless image/video transmission, space communications, advanced channel coding techniques, and B5G wireless transmission technologies.

Rongxing Lu (Fellow, IEEE) received the Ph.D. degree from the Department of Electrical and Computer Engineering, University of Waterloo, Waterloo, ON, Canada, in 2012.

He is a Mastercard IoT Research Chair, a University Research Scholar, and an Associate Professor with the Faculty of Computer Science (FCS), University of New Brunswick (UNB), Fredericton, NB, Canada. Before that, he worked as an Assistant Professor with the School of Electrical and Electronic Engineering, Nanyang Technological University, Singapore, from April 2013 to August 2016. He worked as a Postdoctoral Fellow with the University of Waterloo, Waterloo, ON, Canada, from May 2012 to April 2013. His research interests include applied cryptography, privacy-enhancing technologies, and IoT-big data security and privacy.

Dr. Lu was awarded the most prestigious "Governor General's Gold Medal," when he received his Ph.D. degree from the Department of Electrical and Computer Engineering, University of Waterloo in 2012; and won the 8th IEEE Communications Society (ComSoc) Asia–Pacific Outstanding Young Researcher Award in 2013. He has published extensively in his areas of expertise, and was the recipient of nine best (student) paper awards from some reputable journals and conferences. He is the Winner of 2016–2017 Excellence in Teaching Award, FCS, UNB. He currently serves as the Chair for IEEE ComSoc Communications and Information Security Technical Committee and the Founding Co-Chair for IEEE TEMS Blockchain and Distributed Ledgers Technologies Technical Committee.

Qinyu Zhang (Senior Member, IEEE) received the bachelor's degree in communication engineering from Harbin Institute of Technology, Harbin, China, in 1994, and the Ph.D. degree in biomedical and electrical engineering from the University of Tokushima, Tokushima, Japan, in 2003.

From 1999 to 2003, he was an Assistant Professor with the University of Tokushima. He has been with Harbin Institute of Technology (Shenzhen), Shenzhen, China, since 2003, where he is currently a Full Professor and serves as the Dean of the EIE School. His research interests include aerospace communications and networks, and wireless communications and networks.

Prof. Zhang has been awarded the National Science Fund for Distinguished Young Scholars, the Young and Middle-Aged Leading Scientist of China, and the Chinese New Century Excellent Talents in University, and obtained three scientific and technological awards from governments.